Annals of Nuclear Medicine (2021) 35:47–58
https://doi.org/10.1007/s12149-020-01534-y

ORIGINAL ARTICLE

Development of a new Python-based cardiac phantom for myocardial SPECT imaging

Osama S. Hanafy[1] · Magdy M. Khalil[2] · Ibrahim M. Khater[1] · Haitham S. Mohammed[1]

Received: 19 June 2020 / Accepted: 19 September 2020 / Published online: 17 October 2020
© The Japanese Society of Nuclear Medicine 2020

Abstract

Purpose The aim of this work was to develop a digital dynamic cardiac phantom able to mimic gated myocardial perfusion single photon emission computed tomography (SPECT) images.

Methods A software code package was written to construct a cardiac digital phantom based on mathematical ellipsoidal model utilizing powerful numerical and mathematic libraries of python programing language. An ellipsoidal mathematical model was adopted to create the left ventricle geometrical volume including myocardial boundaries, left ventricular cavity, with incorporation of myocardial wall thickening and motion. Realistic myocardial count density from true patient studies was used to simulate statistical intensity variation during myocardial contraction. A combination of different levels of defect extent and severity were precisely modeled taking into consideration defect size variation during cardiac contraction. Wall thickening was also modeled taking into account the effect of partial volume.

Results It has been successful to build a python-based software code that is able to model gated myocardial perfusion SPECT images with variable left ventricular volumes and ejection fraction. The recent flexibility of python programming enabled us to manipulate the shape and control the functional parameters in addition to creating variable sized-defects, extents and severities in different locations. Furthermore, the phantom code also provides different levels of image filtration mimicking those filters used in image reconstruction and their influence on image quality. Defect extent and severity were found to impact functional parameter estimation in consistence to clinical examinations.

Conclusion A python-based gated myocardial perfusion SPECT phantom has been successfully developed. The phantom proved to be reliable to assess cardiac software analysis tools in terms of perfusion and functional parameters. The software code is under further development and refinement so that more functionalities and features can be added.

Keywords Mathematical phantoms · Python · Cardiac SPECT · Simulation · Left ventricle

Introduction

Myocardial perfusion single photon emission computed tomography (SPECT) has a well-established position among cardiac imaging modalities. The availability of simulated gated myocardial perfusion SPECT images with specific abnormalities has several benefits in providing easy alternatives but viable options in image reconstruction and evaluation of cardiac software packages. There have been lots of advances in the anthropomorphic human phantoms in the last two decades [1, 2]. These developments have several implementations in nuclear medicine applications including image acquisition, reconstruction, data analysis, calibration, quality assurance and quality control, radiation dose calculation and radiation protection purposes [3–7].

Generally, there are 2 types of phantoms, namely numerical and non-numerical phantoms. Numerical phantoms include stylized (i.e. Mathematical-based), voxel-based (i.e., Tomographic imaging-based), and hybrid-based phantoms. Non-numerical phantoms are those that use solid geometries and inserts [1, 2]. Stylized phantoms are those which first

Electronic supplementary material The online version of this article (https://doi.org/10.1007/s12149-020-01534-y) contains supplementary material, which is available to authorized users.

✉ Magdy M. Khalil
magdy_khalil@hotmail.com

[1] Department of Biophysics, Faculty of Science, Cairo University, Cairo, Egypt

[2] Department of Physics, Faculty of Science, Helwan University, Cairo, Egypt

developed by ORNL (Oake Ridge National Laboratory) and represent the human anatomy using mathematical equations based on analytical geometries, such as plane, cylinder, elliptical, conical and spherical surfaces. Voxel phantoms are based on 3D imaging techniques, such as MRI or CT or sectional color phantoms, from patients that are made by manual or semi-automatic segmentations of tissues. They are more realistic than the stylized phantoms.

There are numbers of software programs that are used in deriving quantitative information from gated myocardial perfusion SPECT. They provide estimates of left ventricle end-diastolic volume (EDV), end-systolic volume (ESV), ejection fraction (EF), phase analysis, wall thickening motion and perfusion parameters, such as defect extent and severity, stress and rest summed scores and total perfusion deficit (TPD) [10–12]. Therefore, there were potential attempts to design cardiac phantoms able to provide realistic structure, dimensions, contractility, and also used to validate quantitative software packages [13].

Python has become one of the most important and multifunctional programming languages in this era. It is a high-level programming. It has easy syntaxes that offer greater flexibility and advantages over some programming languages, such as C, C++ and Java [16].

The aim of this study was, therefore, to design a computational cardiac phantom for SPECT imaging as flexible platform simulating the interfering parameters of myocardial wall thickness, volume, count variation and cardiac defect extent with deferent degrees of severities.

Materials and methods

We have utilized some powerful scientific libraries, such as numpy and scipy, to build the phantom in a slice-by-slice manner and used the matplotlib library to visualize and test the generated myocardial volume. Then, the pydicom library was used to convert the python produced images into dicom format so that it can be read by the scanner cardiac software package.

Numpy

The numpy library enjoys several computational features including multi-dimensional array, sophisticated functions, tools to integrate C/C++ and Fortran code. It has also useful linear algebra, Fourier transform, and random number capabilities [17].

Scipy

SciPy is also very useful mathematical tool and contains modules for optimization, linear algebra, interpolation, integration, fast Fourier transform (FFT), image and signal processing, ordinary differential equation solvers and many other functions in science and engineering.

Phantom design

The phantom has been designed based on the well-known elliptical model that was used extensively in the literature [11, 18, 19], see Fig. 1. The whole volume was divided into multiple consecutive slices taking into consideration the decreasing and increasing length of the short and long axes of the adjacent consecutive myocardial slices. The equation of the elliptical model is represented as follows:

$$\frac{(x-h)^2}{b^2}+\frac{(y-k)^2}{a^2}=1. \quad (1)$$

x: radius of ellipse at point y.

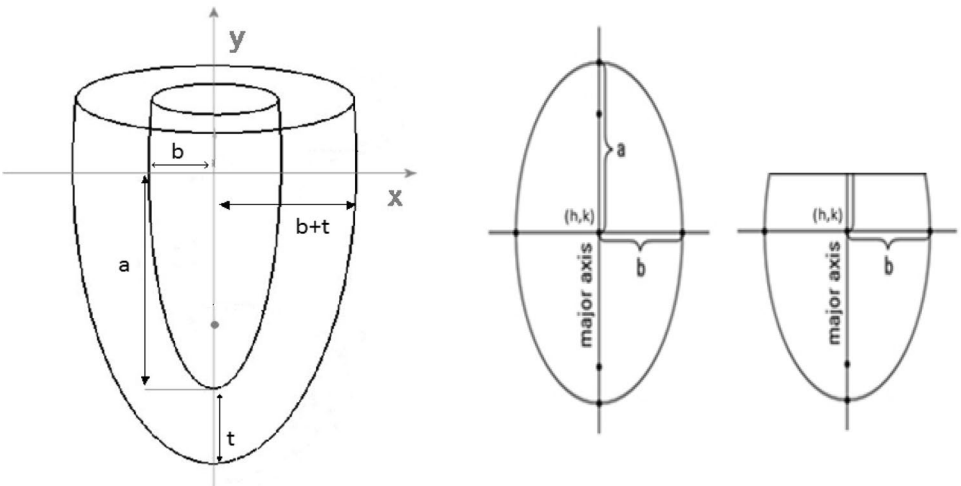

Fig. 1 The elliptical shape used in developing the heart geometry using the mathematical libraries of the python software program. a and b are constants for each ellipse. This equation was initially used for endocardium whereas for epicardium the constants a and b were modified with a + t and b + t where t is the wall thickness. The figure shows an extra portion (half ellipse + extra basal portion) which accounts for the valve, this adds some reality to the simulation

(h, k): center point of ellipse.

b: radius of base (max radius).

a: long axis (max long axis).

a and b are constants for each ellipse. This equation was initially used for generating the endocardial boundaries whereas the epicardium was simulated by adding the myocardial thickness t to the constants a and b (i.e. $a+t$ and $b+t$) where t is the wall thickness.

The individual slices were stacked together to form a one-time point of full cardiac volume. These individual volumes were then stacked to generate a complete cardiac cycle. Each slice has undergone a chain of processing to control the mid-myocardial counts, standard deviation of count distribution, wall thickness, volume of the left ventricle, and also extent and severity when a hypoperfusion defect is sought for simulation. The most important issue was the variation of all these parameters during the cardiac cycle (gates), and this was the most complex task.

The maximum short axis (the radius of myocardial base) and long axis of the ellipse were used as initial inputs to build up individual and consecutive short axes that construct the whole volume. Then, this output was used as an input to another function called slice_maker (defined in the appendix) that integrate this information in addition to other parameters that control thickness, mid count, standard deviation to reveal one cardiac slice. An iteration loop is also used to build up one particular volume at certain one-time point. Repeating this process over the standard cardiac cycle provides a full dynamic version of myocardial perfusion images. The slice-maker function also handles the number of gated time points so that 16 or higher order of temporal data can be sampled. The mid count was extracted from normal subjects who have undergone SPECT examination for likelihood of coronary artery disease and diagnosed with negative results. The mid-myocardial count was taken as the mean value with variation equivalent to 95% confidence interval (i.e. SD = ± 2).

To simulate the random noise associated with radioactive decay, the Poisson function was used to provide statistical count variation across the simulated images. The functional form of the Poisson noise model used was:

$$P_k(\text{n events in interval}) = e^{\lambda}\frac{\lambda^n}{n!}$$

λ: is the average number of events per interval.

e: is the constant 2.7182 (Euler's number).

n: takes values 0,1, 2,.. etc.

Another important routine was applied to create hypoperfusion defects throughout a given myocardial thickness over one or more slices based on defect volume (i.e. extent). For example, five different defects were made with extent of 10%, 20%, 30%, 40%, and 50% of the left ventricle volume each with 5 different severities of values 90%, 80%, 70%, and 60% of the mid-myocardial count. For example, the phantom with 10% extent and 70% severity means that it has a defect that represents 10% of the left ventricular size and hypoperfusion of 30% of the mid-myocardial count. Notice that the maximal counts are often in the mid-point due to point spread function response.

The parameters a and b in (Eq. 1) were so instrumental in controlling the volume of the myocardium. To simulate heart motion and muscle contractility, eight volumes were constructed representing the time–volume curve such that each volume represented one gate (i.e. single time point) in the cardiac cycle. The volume variation between these 8 volumes was made similar to the first half of the cosine function.

Myocardial count distribution was made such that the mid-myocardial count has the maximum value that gradually decreases when moving towards the periphery of the myocardium. This pattern of count variation was simulated following Gaussian function as it typically shows maximal uptake in the middle with symmetric count decline in both sides. This is consistent with radial count profiles but not in exact agreement due to some asymmetry especially at the endocardial side owing to count spill-over and count contamination in the cavity portion of the count profile [20].

For determination of myocardial thickening, the partial volume phenomenon associated with myocardial contraction was employed. In this regard, the apparent cardiac walls do increase and decrease in intensity during systole and diastole in proportion to myocardial thickening [21]. To simulate this process in a more realistic manner, ten patients who have undergone myocardial perfusion SPECT imaging were analyzed through circumferential profile drawn over the mid-myocardial wall and polynomial function was used in data fitting:

$$Y = 0.235x^3 - 3.556x^2 + 14.32x + 21.78,$$

where x represents the myocardial gate number and y represents the associated change in counts. Figure 2 shows the average counts plotted versus the gate number of the analyzed dataset. The number of circumferential profiles drawn was 60 that extends from the center of the short axis to beyond the extracardiac space. The maximum, average and standard deviation of the recorded counts were calculated. The same equation was used to control the variation in thickness during cardiac cycle with respect to the mid-myocardial count.

The software code was designed in a way that permits one to implement defects in the phantom with different measure of extent (i.e., lesion size) and severity (i.e., reduction in count intensity) as well as defect location within cardiac walls, representing the required defect of the total ventricular volume.

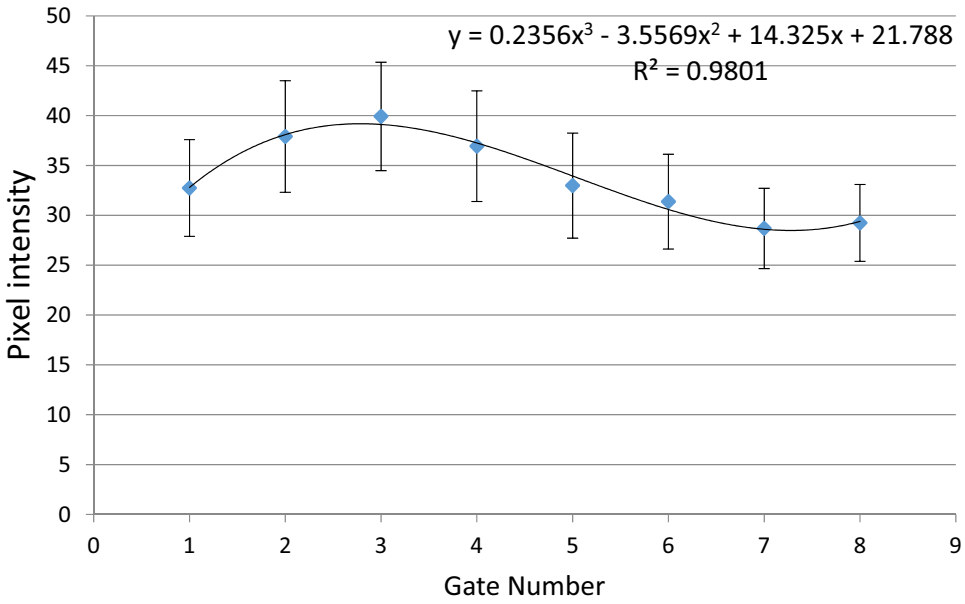

Fig. 2 Shows the average counts plotted versus the gate number of the analyzed normal dataset. A Circumferential profile was measured for the maximum counts of 60 radial rays drawn from the mid-short axis to points beyond the myocardial wall. The maximum counts was then derived and the average and standard deviation was calculated for the randomly selected routine patients

In order to insert a defect in specific location with specific degree and size, first we select the location by specifying the range of voxels in which the defect will be implemented. For example, if we want a defect in mid anterior wall, we target voxels that lie within the sector (~ 10–2 o'clock) in the mid slices of the phantom. A counter function is used to register those voxels that belong to that part so that this information is transferred to another routine of the code to handle the count density to achieve the required level of severity. See "defect-maker" function in the Appendix.

This feature is important as myocardial defect can be arbitrarily simulated at any location with wide range of defect size and severity. It is useful when attempts are made to evaluate the performance of quantitative algorithms in myocardial perfusion imaging in terms of accuracy, influence of defect size and location, as well as determination of functional parameters and in comparative studies looking at the relative performance of different methods [22].

Finally, we used the Digital Imaging and Communication in Medicine (DICOM) implementation function to sort out the generated slices and made them readily loaded by the Quantitative Gated SPECT (QGS) software package (Cedars-Sinai medical center, California, USA). The appendix contains explanation of program flow, classes, functions, parameters similar to what is called pseudocode of the script used in phantom development.

Phantom cine motion

Heart wall motion and thickening can be only seen when different gates that represent volume change of the myocardium are sequentially displayed. The software enables users to create sub-volumes (DICOM file format) that represent for example eight gates each sub-volume differs from the other in wall thickness, volume and mid-myocardial count based on blood volume changes within cardiac cavity. This has been implemented by altering the mathematical parameters of the ellipsoidal model as described earlier. When the dynamic volume was loaded through QGS software package, it was possible to visualize the phantom myocardial motion and wall thickening as shown in the results as well as the attached supplement**.**

Applications

Three different simulations were used as template to create diseased myocardium with different extent and severity in the anterior wall. The range of simulated defect extent was from 10 to 50% of the total myocardium and for each extent there were five levels of defect severity ranging from 90 to 50% in a step of 10%. The results of this step were three simulations times 5 levels of extent times five levels of defect severity. These combinations resulted in 75 diseased myocardial phantom model. Furthermore, simulation two described in (Table 1) was used to create 3 levels of statistical count variation so that count statistics could be

Table 1 Simulation values of left ventricular volumes (EDV and ESV) and ejection fraction (EF) that have been used in simulation studies of the developed phantom

	Simulation 1	Simulation 2	Simulation 3
EDV (ml)	108	101	102
ESV (ml)	75	54	63
EF (%)	31	47	38

investigated. The count variation among the beating slices was made to follow polynomial function derived from normal subjects as outlined earlier.

Similarly, image filtration during reconstruction could also potentially impact myocardial perfusion and function quantification. Simulation 2 was also used applying 3 different levels of Gaussian filtration at sigma (σ) value of 0, 1 and 2. Sigma is the standard deviation of Gaussian kernel (i.e., spatial smoothing filter). The Gaussian function used in image filtration was defined as:

$$G(x,y) = \frac{1}{2\pi\sigma^2} e^{-\frac{x^2+y^2}{2\pi\sigma^2}}.$$

where x and y are location of pixels on which Gaussian mask would be applied. G (x, y) is the filtered pixel value after application of Gaussian mask [23].

All phantoms generated above were used to assess variations associated with many of myocardial perfusion and function parameters including EDV, ESV, EF, summed motion score (SMS), summed thickening score (STS), summed thickening percent (ST%), peak filling rate (PFR), time to peak filling (TTPF), mean filling rate over the first third of the end-systolic to end-diastolic phase (MFR/3), motion extent (Mot Ext) and thickening extent (Thk Ext).

Statistical analysis

Continues variables were represented as mean ± SD. To draw a general conclusion of the performance of the phantom, the simulation results performed were averaged in terms of defect severity and also with respect to defect extent over the three numerical simulations. Since the true values are known in advance, we were able to calculate the % difference between the simulation results and the ground truth. A p value less than 0.05 was considered statistically significant. The statistical package for social sciences was used in data analysis (IBM SPSS, Armonk, NY, version 22).

Results

The QGS software has been used to view the phantom images and record the anatomical and functional parameters for each simulation. The phantom code was able to produce myocardial slices with gating features in consistence with routine myocardial perfusion SPECT images. The simple nature of the code as well as the quick interpretation capability of the python programing language all have made the execution process very reasonable and does fit well in any clinical research environment.

As an example to show the created myocardial perfusion and gating slices, Fig. 3 displays horizontal, vertical and short axis images at two different phases namely end diastole and end systole. One can also notice the myocardial surface rendering of the simulated volume at the same kinetic phases. The same figure demonstrates how the phantom was successfully able to provide an anatomically relevant shape of left ventricular walls and myocardial cavity viewed in the standard format [24]. The count variation due to myocardial thickening is also apparent due to partial volume effect. The top row images were inserted for comparative purposes.

Figure 4 shows images created using the developed phantom displaying a variety of defects with severity of 70%, 90% and 100% all produced at an extent of 20%. It is obvious that as the defect severity increases, the defect count decreases in proportion. The vertical long axis mages are also demonstrated.

Figure 5 depicts bull's eye of myocardial perfusion slices created using the newly developed software with extent of 30% and severity of 60% along with the corresponding thickening and motion polar maps. Notice that for the left side images, the software code was able to address the phenomenon of intensity variation in both end diastole and end systole due to cardiac contraction simulating effects of partial volume phenomenon.

The mean EDV, ESV and EF averaged over the three simulations measured for a number of clinically relevant defect extent (10–50%) and severity (50–90%) are shown in Fig. 6. A closer look into the inserted table of the same figure, one can notice that the results are consistent with the fact that the performance of the software algorithm may be reduced in presence of large perfusion defects [22, 25]. Table 2 shows the recorded values using the newly developed phantom versus those reported in clinical examinations for determination of diastolic function parameters [28–31, 32].

Figure 7 displays the percent difference between the true and average values of perfusion and functional parameters measured for the three different simulation of the left ventricular volumes. The average values were taken over an extent of 10–50% each with severity range of 50–90%. It is apparent that perfusion and functional parameters were significantly affected in a similar manner to that observed in true clinical setting.

Figure 8 shows the % difference between the true and average values of functional parameters for 3 different levels of a low pass filter (FWHM = 1, 2 and 3 sigma). Image smoothing serves to reduce ventricular cavity and spread the myocardial wall thickness into larger area. These features hinder the computational algorithm to delineate the endocardium and epicardium with high precision as demonstrated in previous reports [31, 32].

Furthermore, simulation of cardiac SPECT studies with different count densities is demonstrated in Fig. 9. There was also a variable response of the functional parameters due to uncertainty associated with low versus high counts

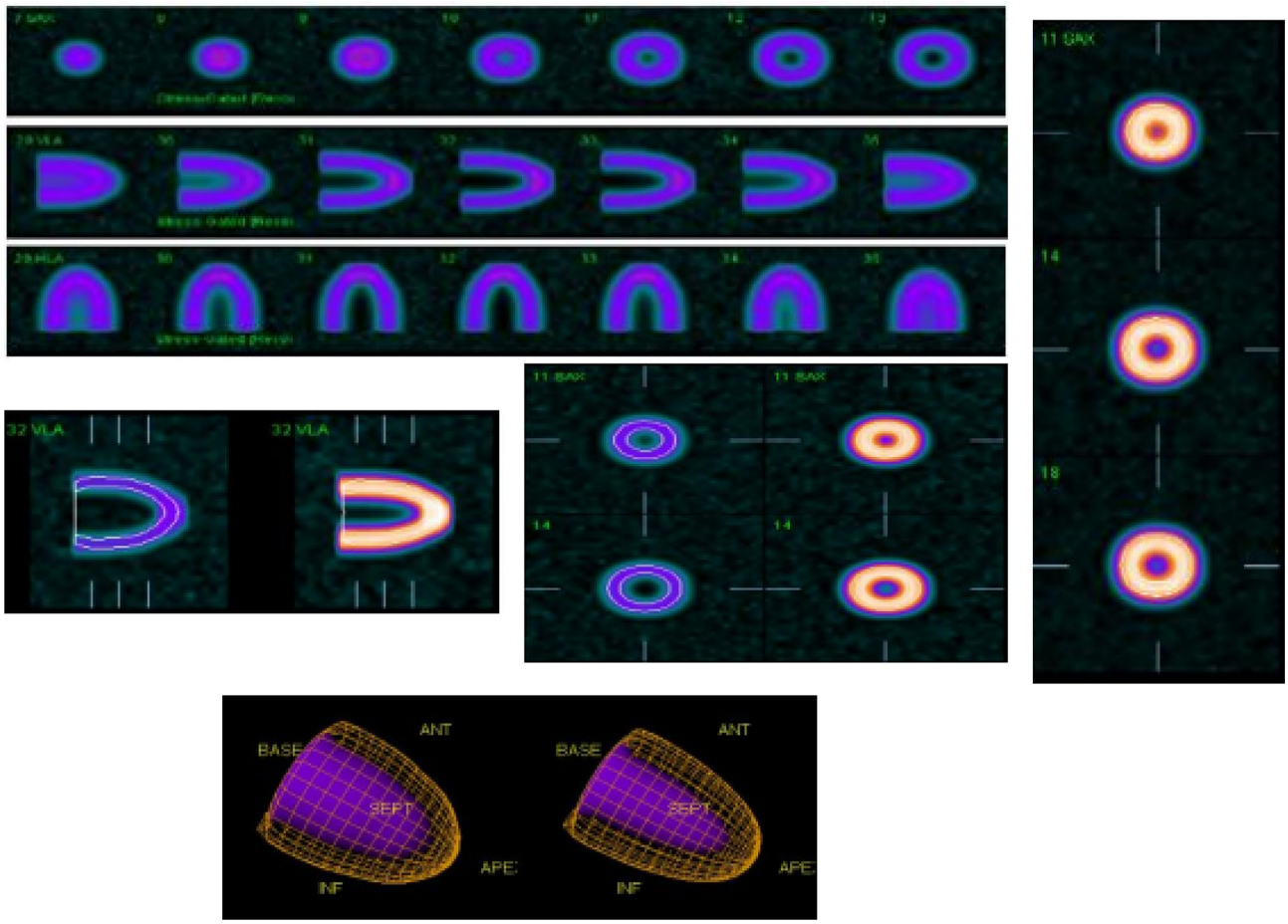

Fig. 3 Representative short, horizontal and vertical long axis slices of myocardial volume created using the newly developed python-based software code. Image display is performed using the QGS software package. The short axis images were taken at end diastole and end systole showing the variation of count density due to partial volume effect. An electronic supplement file is provided to show the cine motion of simulated phantom

statistics that could confound the performance of the quantitative algorithms in parameter estimation [33].

Discussion

The Python programming language has powerful scientific libraries that enabled us to design a program script that can produce a digital cardiac phantom using a personal computer with humble capabilities. The current version of the code was run using Intel Pentium B960@2.20 GHz, RAM of 2 GB Single-Channel running on Windows 7. These settings allowed to mimic the left ventricle and its complicated nature in addition to simulating hypoperfused myocardial segments with various extent, severity and locations.

Myocardial perfusion imaging using SPECT technologies has recently been advanced on many levels of hardware architecture and software implementation. These developments included data acquisition, reconstruction and image analysis [34, 35]. The availability of myocardial SPECT images of simulated patient studies provides unique opportunities to investigate critical parameters that potentially impact image quality and quantitative accuracy. Moreover, additional gain is obtained when features of abnormalities are precisely modeled [13, 36]. While the phantom could be readily modified to simulate cardiac PET data, the use of this phantom in PET imaging would require further refinement to account for differences in spatial resolution and signal-to-noise ratio.

The results showed the capability of the developed software code to model myocardial SPECT images with high accuracy in terms of perfusion and functional characteristics for subjects undergoing gated myocardial SPECT. The heart contractility and count variation across time bins was also incorporated to add dynamic features to the simulation model. The count distribution within each gate and relative increase and decrease among gates were also considered during heart motion. The change in ventricular volume

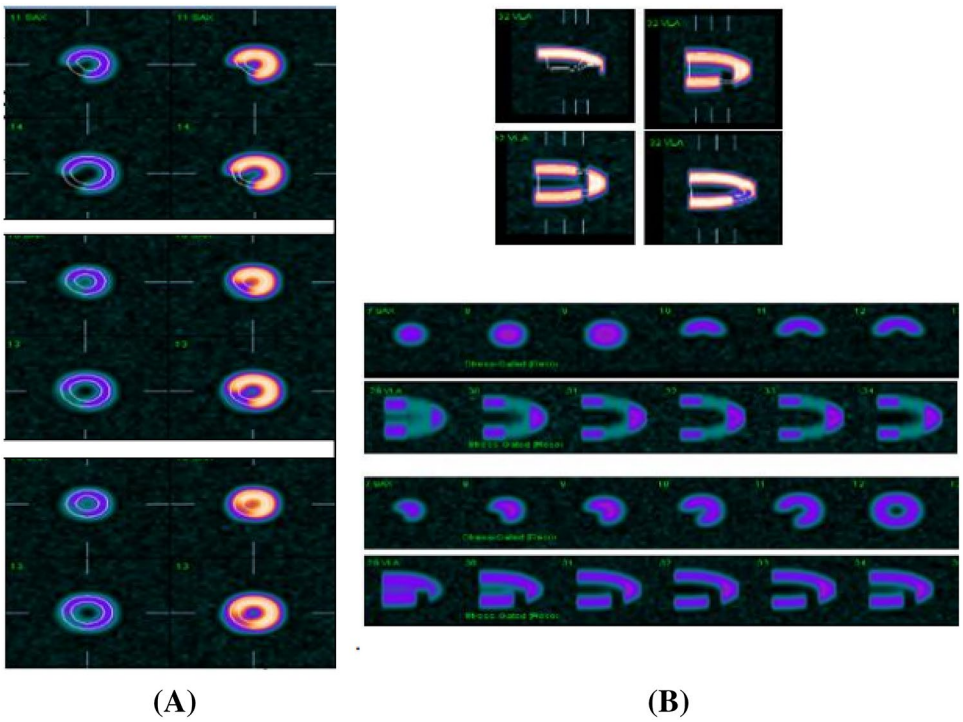

Fig. 4 A collection of images created using the developed phantom showing a variety of defects with different severities (100%, 90%, and 70% from top to bottom) and fixed extent (20%) on the short axis images as indicated in (**a**) where count reduction is gradually observed as defect severity increases. The corresponding vertical long axis mages are displayed on the right panel (**b**)

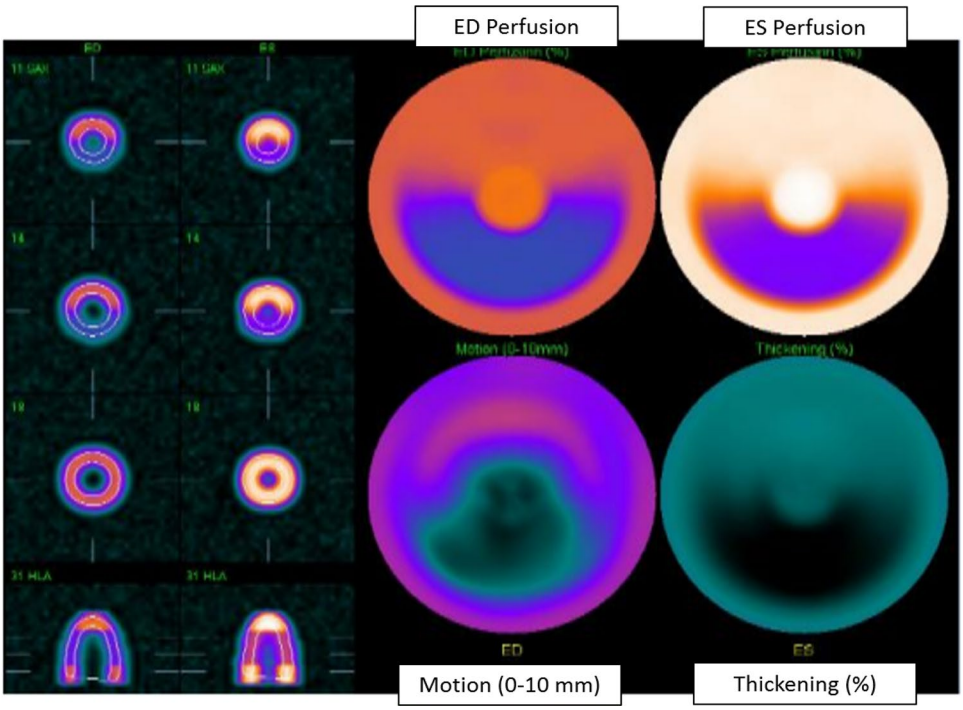

Fig. 5 Polar map for myocardial perfusion slices created using the newly developed python code with extent of 30% and severity of 60% along with the corresponding thickening and motion maps. Notice that for the left side images, the software code was able to address the phenomenon of intensity variation in both end diastole and end-systole due to cardiac contraction and associated partial volume effect

during systole and diastole was also dealt with in the execution of the software code. These characteristics provided an overall acceptable performance of the new proposed heart model as illustrated in the results section.

Perfusion defects are crucial parameters when attempts are made to model SPECT images derived from cardiac studies. The flexibility of the code has been instrumental to implement cardiac defects with specific size (extent) and count reduction (severity) in different locations in the left ventricle. Although the defect extent and severity are distorted during left ventricular contraction, this feature has been resolved such that the severity and extent are

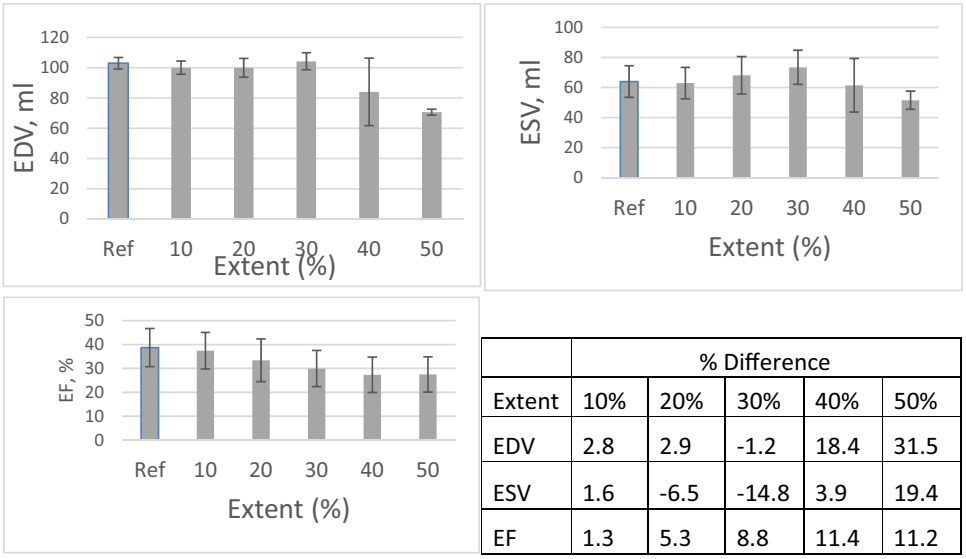

	% Difference				
Extent	10%	20%	30%	40%	50%
EDV	2.8	2.9	-1.2	18.4	31.5
ESV	1.6	-6.5	-14.8	3.9	19.4
EF	1.3	5.3	8.8	11.4	11.2

Fig. 6 The mean EDV, ESV and EF averaged over the range of defect severity as well as across the 3 different simulations of the left ventricles for lesion extent of 10–50%. The first column in all graphs is the reference phantom values (i.e., without a defect). The lower right table records the % difference between the average values of the three functional parameters plotted in the graphs and the reference values. The range of % difference is consistent with clinical findings where an underestimation of 32% can be seen in patients with large perfusion defects

Table 2 Simulation and true values of the most important diastolic function parameters as reported by the newly developed cardiac phantom for the 3 different simulations with a clinical range of defect extent and severity

	PFR (EDV/s)	MFR/3 (EDV/s)	TTPF (ms)
Truth	2.01	1.38	98
Sim1	1.65	1.03	92.48
Truth	2.70	1.70	90.00
Sim2	2.51	1.50	87.76
Truth	1.15	0.74	164.00
Sim3	0.91	0.65	127.40
Avg Simulation	1.69 ± 0.80	1.06 ± 0.42	102.55 ± 21.65
Patients (literature)	2.6 ± 0.46*	Range [1–2]$^{\$}$	165.2 ± 23.1*
	$2.32 \pm 0.4^{\&}$	$(1.95 \pm 0.48)^{\&}$	Range [100–550]$^{@}$
	2.4 ± 0.52^{M}	1.49 ± 0.32^{M}	169 ± 27^{M}
	2.87 ± 0.63^{F}	1.65 ± 0.33^{F}	161 ± 28^{F}

The parameters of Sim1, Sim2, and Sim3 are those described in Table 1

The superscripts M and F refer to male and female normal limits respectively

*[28], $^{\&}$[29], $^{\$}$[30], $^{@}$[31], ^{M,F}[32]

maintained in proportion to the myocardial wall volume. This permits one to evaluate the accuracy of the computational algorithms in delineating myocardium and extracting quantitative measures.

The various simulations performed have provided consistent results with those reported in clinical studies. The increased defect extent of myocardial SPECT images is associated with gradual failure of the quantitative algorithms to replicate the true values. This has been observed when the phantom images were used to investigate the role of defect extent and severity on calculations of the left ventricular volumes and ejection fraction. The process of contouring requires a high contrast myocardial boundaries and, hence, an underestimation of 32%, 19%, and 11% in EDV, ESV and EF, respectively, was found in defect extent of 50% [37].

On the other hand, the % difference was not great in simulations results of small perfusion defects. The variation observed represented by % difference due to images filtration and count statistic have also resulted in alteration of functional parameters in line with those measures encountered in practice. Moreover, absolute measure of diastolic functions including PFR and TTPF was found of very close clinical relevance as shown in Table 2.

Nevertheless, it is important to stress on the noise model used in phantom generation. The Poisson function is one of the commonly used noise models due to the random nature of radioactive decay but does not necessarily represent how noise is corrupted during several steps of data acquisition and image reconstruction. This could add further complexity to the generated myocardial slices and depends to large extent on gamma camera imaging system. Future developments of this phantom would consider different and more realistic noise models.

While the mathematical phantoms are no longer the state-of-the-art models in simulating heart anatomy and physiology, there is still room for its utility in many aspects of cardiac SPECT imaging including evaluation of perfusion and functional parameters as well as the possibility of adding image degrading factors of attenuation, scatter and resolution effects. Those phantoms are also simple, flexible and can be easily modified to reflect patient size.

The developed phantom is under intensive development and it is planned to include cardiac dyssynchrony in the ventricular volume so that evaluation of phase analysis and

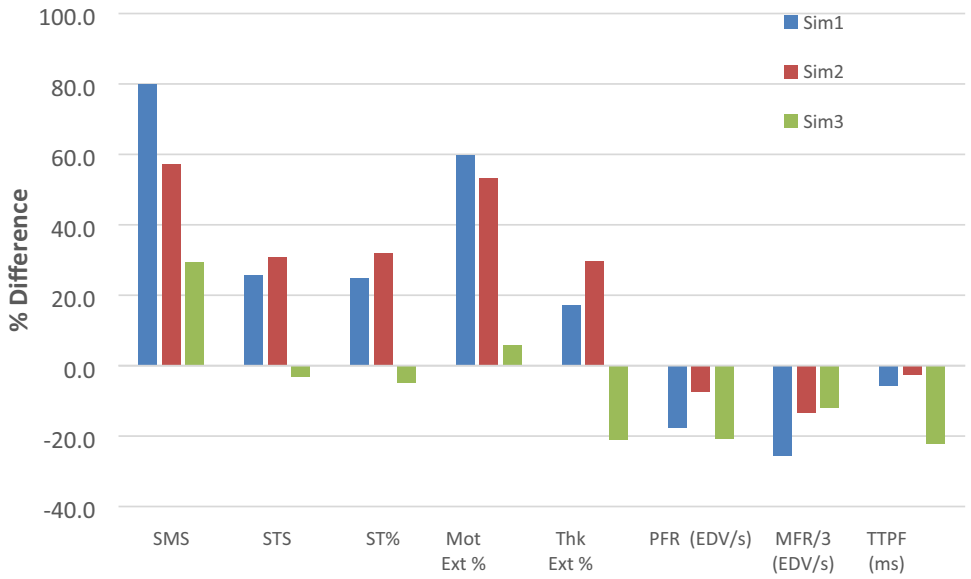

Fig. 7 The % difference between the true and average values of perfusion and functional parameters for the 3 different simulation of the left ventricular volumes. The average values were taken over an extent of 10–50% each with severity range of 50–90%. It is clear that altering the myocardial cavity volume results in concomitant changes in measurement of many of the tested parameters consistent with those changes commonly seen in clinical investigations. Parameters of sim1, sim2 and sim3 including left ventricular volume and ejection fraction are described in Table 1. *Abbreviations:* summed motion score (*SMS*), summed thickening score (*STS*), summed thickening percent (*ST%*), peak filling rate (*PFR*), time to peak filling (*TTPF*), mean filling rate over the first third of the end-systolic to end-diastolic phase (*MFR/3*), motion extent (*Mot Ext%*) and thickening extent (*Thk Ext%*)

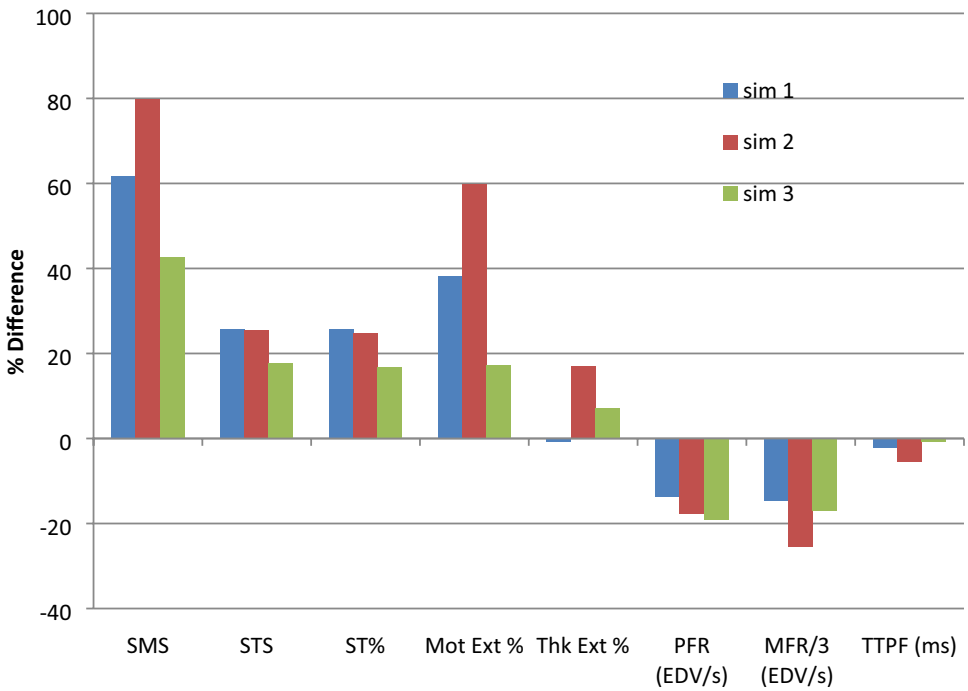

Fig. 8 The % difference between the true and average values of simulated myocardial parameters for three different levels of low pass filtration (FWHM = 1, 2 and 3 sigma). This variance is consistent to what seen in clinical studies. *Abbreviations:* summed motion score (*SMS*), summed thickening score (*STS*), summed thickening percent (*ST%*), peak filling rate (*PFR*), time to peak filling (*TTPF*), mean filling rate over the first third of the end-systolic to end-diastolic phase (*MFR/3*), motion extent (*Mot Ext%*) and thickening extent (*Thk Ext%*)

testing the computational capability of cardiac algorithms can be carried out. Attempts are also sought to voxelize the phantom providing opportunities to use in Monte Carlo simulation including imaging and dosimetric applications. There are also some important features that are underway including development of user interface (i.e., GUI) providing the user with a greater flexibility in cardiac simulation. Additional features are also sought including the insertion of

Fig. 9 The % difference between the true values and average myocardial functional parameters for three different count levels simulated using the developed cardiac phantom. *Abbreviations:* summed motion score (*SMS*), summed thickening score (*STS*), summed thickening percent (*ST%*), peak filling rate (PFR), time to peak filling (*TTPF*), mean filling rate over the first third of the end-systolic to end-diastolic phase (*MFR/3*), motion extent (*Mot Ext%*) and thickening extent (*Thk Ext%*)

the cardiac phantom in chest region with surrounding tissues and organs as well as gender-based anatomies. Furthermore, another area of our interest is the addition and simulation of coronary trees in the phantom model.

The phantom developed in this study proved useful offering flexible control over parameters that specify the shape, defect location, size, severity, acquired count statistics, image noise and reconstruction filters. In the new era of artificial intelligence and deep learning, a user-friendly software package could immensely facilitate the production of large dataset of myocardial slices with different characteristics enabling, for example, myocardial segmentation, defect detection, determination of left ventricular volumes and ejection fraction. We believe that our software package would play a significant role in this significant area of research and development.

Acknowledgment The authors disclose that they do not have any conflict of interest. All authors would like to express their gratitude to the editor and reviewers for their time and efforts made to the manuscript. The software code will be released in the public domain and until that time it is available upon request from the corresponding author.

Appendix

Code structure, function and parameters

class SPECT.oop_model.Gate (index, maxthick, maxcount)

The class Gate creates a gate of the heart cycle with specific parameters that are specific for each gate

defect_maker (*gate*, *start*, *slices_to_be_modified*, *extent*, *severity*)

Making defects in each volume of each gate with specific size (extent) and degree (severity)

Parameters	Gate – a list of images of specific gate Start – the index of first slice that will be modified Slices_to_be_modified – no. of slices that will be modified Extent – extent Severity – severity

Dicom_implementation (*slices*, *gateslices*, *base_repeation*, *path*, *name*, *start*, *slices_to_be_modified*, *extent*, *severity*)

Very important function for implementation of generated images in the software with dicom format with specific dicom headers

Parameters	Slices – number of all generated slices that need to be implemented Gateslices – number of slices in each gate Base_repeation – number of repeated myocardial base images Path – path of slices that need to be implemented Name – patient name _as you want to name it

The rest of the arguments are used by the previous functions and defined in the docstrings of these functions

elipse(*y_point*, *endo_long_axis*, *base_radius*)

the function used to produce shape

Parameters:	**y_point** – y_point **Endo_long_axis** – max long axis value (distance from base to apex) **Base_radius** – max short axis value (diameter of base)
Return output:	The x_point related to the inserted

Gray_scale_converter (*imgno*)

Modification of slices that are grey scale_converted by reverse the grey scale of them ‘before dicom implementation

Parameters:	**Imgno** – image _slice name
Return output:	The same image with grey scale reversed

noise_maker (*gate*)

Generating poisson noise in the empty pixels of each image

Parameters:	**Gate** – a list of images of specific gate
Return output:	A list of images of specific gate with noised background

Poisson (*lampda*)

generating randomly distributed Poisson series used for noise.

Parameters:	lampda – the standard deviation of the series

Slicemaker (*r1*, *r2*, *x_var*, *k*, *SD*, *points*, *num*, *midcount*)

used to make each slice

Parameters:	r1 – outer circle diameter. r2 – inner circle diameter. x_var – increment between mini_circles that produce each circle variation in r1 and r2. k – initial count of mini circles. SD – standard deviation of the iscount function that used to make counts in each slice iscount distributed. Points – related to number of mini_circles used to produce each slice. Num – numerator to name images when saving them. Midcount – mid_myocardial count of a volume
Return output:	Of this function is one gate with specific parameters

Smoothing_maker(*gate*, *sigma = 1*, *order = 0*, *mode = 'constant'*, *cval = 0.0*)

to make smoothing _but before adding noise with sigma = 1, order = 0,mode = constant.

Parameters:	Gate – a list of images of specific gate in shape of 2d matrix. Sigma – standard deviation for Gaussian kernel. The standard deviations of the Gaussian filter are given for each axis as a sequence, or as a single number, in which case it is equal for all axes. Order – {0, 1, 2, 3} or sequence from same set. The order of the filter along each axis is given as a sequence of integers, or as a single number. An order of 0 corresponds to convolution with a Gaussian kernel. An order of 1, 2, or 3 corresponds to convolution with the first, second or third derivatives of a Gaussian. Higher order derivatives are not implemented. Mode – {‘reflect’, ‘constant’, ‘nearest’, ‘mirror’, ‘wrap’}, optional. The mode parameter determines how the array borders are handled, where cval is the value when mode is equal to ‘constant’. Default is ‘reflect’. cval – scalar, optional Value to fill past edges of input if mode is ‘constant’. Default is 0.0
Return output:	List of images of specific gate _after smoothing in shape of 2d matrices

Starter()

used to generate some empty images required for implementation in the software

used_pixels_counter(*gate*)

counter of the used pixels of images _non zero _pixels in images useful for accurate volume calculation used before adding noise

Parameters:	Gate – a list of images of specific gate

References

1. Xu XG. An exponential growth of computational phantom research in radiation protection, imaging, and radiotherapy: a review of the fifty-year history. Phys Med Biol. 2014;59(18):R233–302.
2. Zaidi H, Xu XG. Computational anthropomorphic models of the human anatomy: the path to realistic Monte Carlo modeling in radiological sciences. Annu Rev Biomed Eng. 2007;9:471–500.
3. Pretorius PH, King MA, Tsui BM, LaCroix KJ, Xia WA. Mathematical model of motion of the heart for use in generating source and attenuation maps for simulating emission imaging. Med Phys. 1999;26(11):2323–32.
4. Könik A, Connolly CM, Johnson KL, Dasari P, Segars PW, et al. Digital anthropomorphic phantoms of non-rigid human respiratory and voluntary body motion for investigating motion correction in emission imaging. Phys Med Biol. 2014;59(14):3669–822.
5. Furhang EE, Chui CS, Sgouros GA. Monte Carlo approach to patient-specific dosimetry. Med Phys. 1996;23(9):1523–9.
6. Bouchet LG, Bolch WE. Five pediatric head and brain mathematical models for use in internal dosimetry. J Nucl Med. 1999;40(8):1327–36.
7. Smith T, Petoussi-Henss N, Zankl M. Comparison of internal radiation doses estimated by MIRD and voxel techniques for a “family” of phantoms. Eur J Nucl Med. 2000;27(9):1387–98.

8. Segars WP. Development and Application of the New Dynamic NURBS based Cardiac-Torso (NCAT) Phantom PhD Dissertation. Carolina: The University of North Carolina; 2001.
9. De Bondt P, Nichols K, Vandenberghe S, Segers P, De Winter O, et al. Validation of gated blood-pool SPECT cardiac measurements tested using a biventricular dynamic physical phantom. J Nucl Med. 2003;44(6):967–72.
10. Khalil MM. Basic Sciences of Nuclear Medicine. London: Springer Science and Business Media; 2010.
11. Germano G, Kiat H, Kavanagh PB, Moriel M, Mazzanti M, et al. Automatic quantification of ejection fraction from gated myocardial perfusion SPECT. J Nucl Med. 1995;36(11):2138–47.
12. Lum DP, Coel MN. Comparison of automatic quantification software for the measurement of ventricular volume and ejection fraction in gated myocardial perfusion SPECT. Nucl Med Commun. 2003;24(3):259–66.
13. Segars WP, Veress AI, Sturgeon GM, Samei E. Incorporation of the living heart model into the 4D XCAT phantom for cardiac imaging research. IEEE Trans Radiat Plasma Med Sci. 2019;3(1):54–60.
14. Khalil MM, Attia A, Ali M, Ziada G, Omar A, Elgazzar A. Echocardiographic validation of the layer of maximum count method in the estimation of the left ventricular EF using gated myocardial perfusion SPECT: correlation with QGS, ECTb, and LVGTF. Nucl Med Commun. 2009;30(8):622–8.
15. Khalil MM, Elgazzar A, Khalil W, Omar A, Ziada G. Assessment of left ventricular ejection fraction by four different methods using 99mTc tetrofosmin gated SPECT in patients with small hearts: correlation with gated blood pool. Nucl Med Commun. 2005;26(10):885–93.
16. Severance C. Python for informatics: Exploring information. Create Space 2013.
17. www.python.org. Accessed on 29 Dec 2019.
18. Wentworth P, Elkner J, Downey AB, Meyers C. How to think like a computer scientist: learning with Python 3. 2012. http://openbookproject.net/thinkcs/python/english3e/. Accessed 29 Dec 2019.
19. www.python.org. Accessed 1 Dec 2019.
20. Van den Broek JHJM, Van den Broek MHLM. Application of an ellipsoidal heart model in studying left ventricular contractions. J Biomech. 1980;13(6):493–503.
21. Domingues JS, Vale MD, Martinez CB. New mathematical model for the surface area of the left ventricle by the truncated prolate spheroid. Sci World J. 2017;1
22. Khalil MM, Elgazzar A, Khalil W. Evaluation of left ventricular ejection fraction by the quantitative algorithms QGS, ECTb, LMC and LVGTF using gated myocardial perfusion SPECT: investigation of relative accuracy. Nucl Med Commun. 2006;27(4):321–32.
23. Gonzalez RC, Woods RE. Digital image processing. USA: Prentice Hall; 2002.
24. Goos P, Meintrup D. Statistics with JMP: Hypothesis Tests. John Wiley and Sons, Newyork: ANOVA and Regression; 2016.
25. Chua T, Yin LC, Thiang TH, Choo TB, Ping DZ, Leng LY. Accuracy of the automated assessment of left ventricular function with gated perfusion SPECT in the presence of perfusion defects and left ventricular dysfunction: correlation with equilibrium radionuclide ventriculography and echocardiography. J Nucl Cardiol. 2000;7(4):301–11.
26. Akincioglu C, Berman DS, Nishina H, Kavanagh PB, et al. Assessment of diastolic function using 16 frame 99mTc-sestamibi gated myocardial perfusion SPECT: normal values. J Nucl Med. 2005;46(7):1102–8.
27. Yoshino T, Nakae I, Matsumoto T, Mitsunami K, Horie M. Relationship between exercise capacity and cardiac diastolic function assessed by time–volume curve from 16-frame gated myocardial perfusion SPECT. Ann Nucl Med. 2010;24(6):469–76.
28. Higuchi T, Taki J, Nakajima K, et al. Left ventricular ejection and filling rate measurement based on the automatic edge detection method of ECG-gated blood pool single-photon emission tomography. Ann Nucl Med. 2004;18(6):507–11.
29. Nakae I, Matsuo S, Tsutamoto T, Matsumoto T, Mitsunami K, Horie M. Assessment of cardiac function in patients with heart disease by quantitative gated myocardial perfusion SPECT. Ann Nucl Med. 2007;21(6):315–23.
30. Kenichi N, et al. Normal values and standardization of parameters in nuclear cardiology: Japanese Society of Nuclear Medicine working group database. Ann Nuclear Med. 2016;30(3):188–99.
31. Véra P, Manrique A, Pontvianne V, Hitzel A, Koning R, Cribier A. Thallium-gated SPECT in patients with major myocardial infarction: effect of filtering and zooming in comparison with equilibrium radionuclide imaging and left ventriculography. J Nucl Med. 1999;40(4):513–21.
32. Hambye AS, Vervaet A, Dobbeleir A. Variability of left ventricular ejection fraction and volumes with quantitative gated SPECT: influence of algorithm, pixel size and reconstruction parameters in small and normal-sized hearts. Eur J Nucl Med Mol Imaging. 2004;31(12):1606–13.
33. Dorbala S, Ananthasubramaniam K, Armstrong IS, Chareonthaitawee P, DePuey EG, et al. Single photon emission computed tomography (SPECT) myocardial perfusion imaging guidelines: instrumentation, acquisition, processing, and interpretation. J Nucl Cardiol. 2018;25(5):1784–846.
34. Piccinelli M, Garcia EV. Advances in software for faster procedure and lower radiotracer dose myocardial perfusion imaging. Prog Cardiovasc Dis. 2015;57(6):579–87.
35. Slomka PJ, Patton JA, Berman DS, Germano G. Advances in technical aspects of myocardial perfusion SPECT imaging. J Nucl Cardiol. 2009;16(2):255–76.
36. Fung GS, Lee TS, Higuchi T, Tsui BM, Segars WP, Veress AI, Gullberg GT. Realistic simulation of regional myocardial perfusion defects for cardiac SPECT studies. IEEE Nucl Sci Symp Conf Rec. 1997;1997(2010):3061–4.
37. Rastgou F, Shojaeifard M, Amin A, et al. Assessment of left ventricular mechanical dyssynchrony by phase analysis of gated-SPECT myocardial perfusion imaging and tissue Doppler imaging: comparison between QGS and ECTb software packages. J Nucl Cardiol. 2014;21(6):1062–71.

Publisher's Note Springer Nature remains neutral with regard to jurisdictional claims in published maps and institutional affiliations.